ACS SyntheticBiology

pubs.acs.org/synthbio

Research Article

# Engineering a PbrR-Based Biosensor for Cell-Free Detection of Lead at the Legal Limit

Holly M. Ekas,[▽] Brenda Wang,[▽] Adam D. Silverman, Julius B. Lucks, Ashty S. Karim, and Michael C. Jewett*

Cite This: *ACS Synth. Biol.* 2024, 13, 3003−3012

Read Online

ACCESS | Metrics & More | Article Recommendations | Supporting Information

**ABSTRACT:** Industrialization and failing infrastructure have led to a growing number of irreversible health conditions resulting from chronic lead exposure. While state-of-the-art analytical chemistry methods provide accurate and sensitive detection of lead, they are too slow, expensive, and centralized to be accessible to many. Cell-free biosensors based on allosteric transcription factors (aTFs) can address the need for accessible, on-demand lead detection at the point of use. However, known aTFs, such as PbrR, are unable to detect lead at concentrations regulated by the Environmental Protection Agency (24−72 nM). Here, we develop a rapid cell-free platform for engineering aTF biosensors with improved sensitivity, selectivity, and dynamic range characteristics. We apply this platform to engineer PbrR mutants for a shift in limit of detection from 10 $\mu$M to 50 nM lead and demonstrate use of PbrR as a cell-free biosensor. We envision that our workflow could be applied to engineer any aTF.

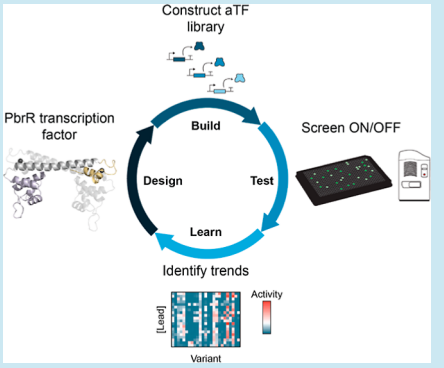


**KEYWORDS:** *cell-free gene expression, synthetic biology, lead, detection, diagnostic, protein engineering*



## INTRODUCTION

Improved point-of-use diagnostics are needed to address the growing crisis of water security, particularly for detecting heavy metals like lead.[1,2] In the United States alone, an estimated 9.2 million lead service lines are in use,[3] with a recent study estimating that 68% of children younger than 6 years old in Chicago are exposed to lead-contaminated water.[4] Lead is regulated in the US at 5−15 ppb (24−72 nM) by the Environmental Protection Agency (EPA).[5] However, state-of-the-art diagnostics that can detect these trace conditions, such as inductively coupled plasma mass spectrometry and flame absorption atomic spectroscopy, are too slow, expensive, and centralized to permit broad water quality monitoring.[1] Thus, a field-deployable lead diagnostic is urgently needed, both to enable households to avoid irreversible health impacts from chronic exposure and to allow public officials to focus finite resources where contamination is the worst.

Freeze-dried, cell-free gene expression (CFE) biosensors[6−9] have shown promise as affordable, sensitive, and easily distributable diagnostic platforms for a range of target analytes such as specific nucleic acids (e.g., SARS-CoV-2,[10] Zika RNA,[11] and Ebola RNA[12]) and small molecules relevant to environmental and human health (e.g., arsenic,[13] pesticides,[14] heavy metals,[15] and fluoride[16]). Decoupled from sustaining life, cell-free, or in vitro, biosensors hold advantages over their whole-cell counterparts, circumventing most biocontainment, cytotoxicity, mass transfer, and instability concerns. However, many sensing elements, such as transcription factors, require engineering to achieve the sensitivity and dynamic range necessary for robust detection at relevant analyte concentrations. The allosteric transcription factor (aTF) PbrR from *Cupriavidus metallidurans* that senses lead falls into this category. Unfortunately, engineering aTFs is complex, owing to multiple conformational states and the need to co-engineer activity in the presence of analyte while maintaining low leak in the absence of a ligand. In vivo selection studies have demonstrated their efficacy with dual positive- and negative-selection schemes, but many still require knowledge of the protein structure of the aTF to narrow their library mutational space.[17−19] Therefore, the precedent for PbrR engineering has been limited, to our knowledge, with one in vivo directed evolution paper that engineered PbrR structures for improved lead selectivity to date.[20]

Here, to address the need for accessible lead diagnostics, we developed a cell-free biosensor to detect lead at the legal limit by engineering PbrR for enhanced sensitivity. To achieve this goal, we created a high-throughput, cell-free platform to optimize aTF-based biosensors. A key feature of our approach is the use of CFE systems to allow for the rapid synthesis and

**Received:** June 26, 2024
**Revised:** August 19, 2024
**Accepted:** August 19, 2024
**Published:** September 10, 2024

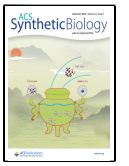

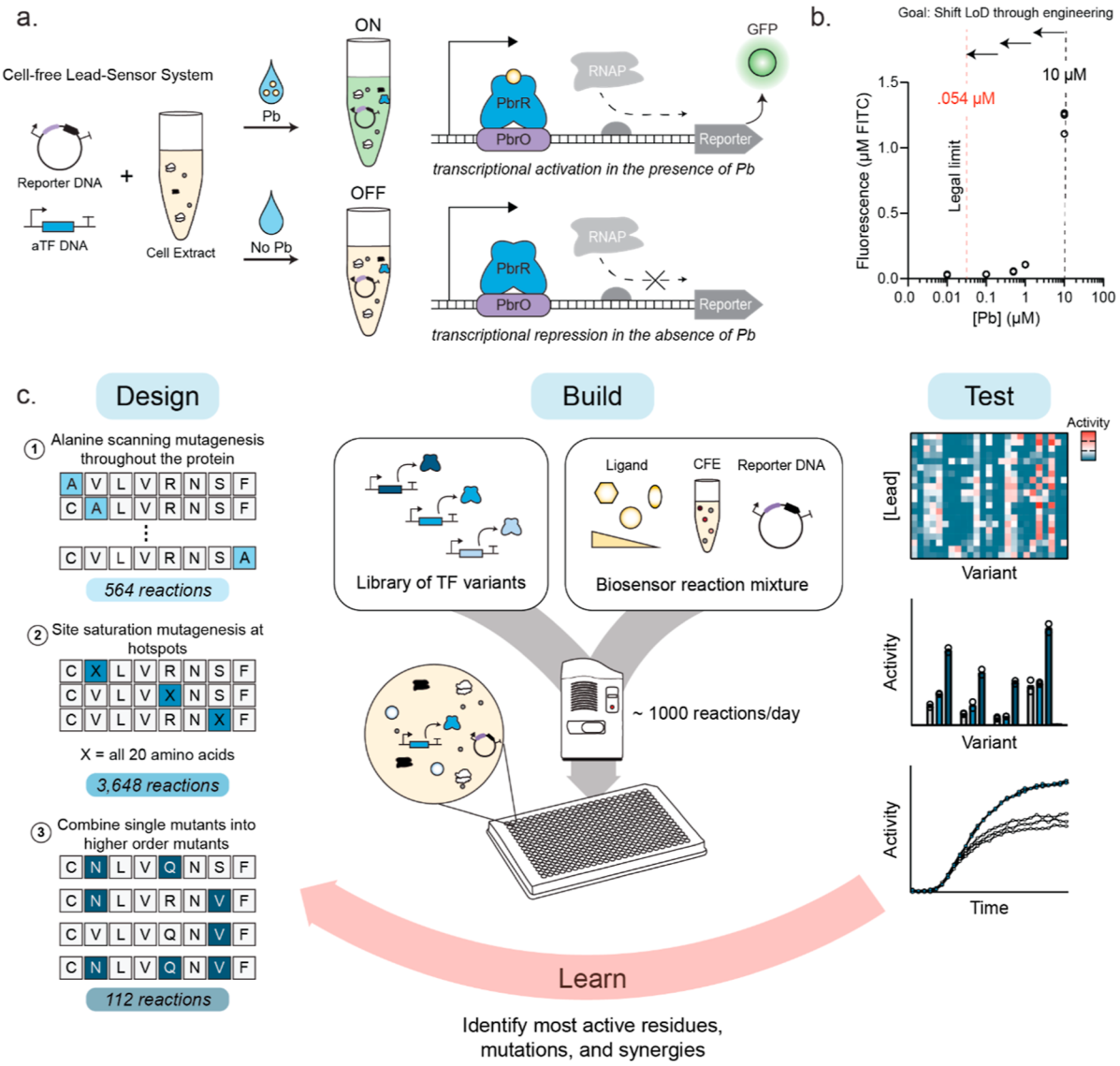


**Figure 1.** A high-throughput cell-free workflow for rapidly engineering PbrR sensitivity. (A) Schematic of PbrR activation mechanism.[22] PbrR binds to the operator site (PbrO). Upon lead binding, PbrR realigns the −35 and −10 operator sequences so that the $\sigma$70 RNA polymerase can initiate transcription. In the absence of lead, the length of spacing between the −35 and −10 sequences prevents transcription by $\sigma$70 RNA polymerase. (B) Dose response curve shows that wild-type PbrR is not sufficiently sensitive to detect lead at the legal limit (0.054 $\mu$M). PbrR has an LoD of 10 $\mu$M. Three technical replicates are graphed individually at 0.01, 0.1, 0.5, 1, and 10 $\mu$M Pb after 15 h. (C) Schematic of iterative workflow for engineering PbrR sensitivity in the cell-free biosensor. (i) Design: protein libraries are designed with the goal of down-selecting the possible search space for engineering sensitivity. First, mutational hotspot residues are identified through an alanine scanning mutagenesis library. Next, site saturation mutagenesis is performed at these hotspots to introduce new functionalities. The best single mutants are then combined into higher-order mutants to identify synergistic effects. (ii) Build: libraries are rapidly assayed using acoustic liquid handling, assembling unique aTF/Pb concentration pairs in each reaction. (iii) Test: fold change can be directly measured from the assay, enabling rapid identification of top variants. Further validations were sometimes performed for higher confidence. (iv) Learn: the top residues, chemistries, and synergies were selected from the assay and used as a starting point for the next iteration of further optimization.

functional testing of mutant aTFs in a design-build-test-learn framework. This framework maps sequence−function relationships for aTF variants with single- and multi-order mutations on analyte limit of detection (LoD), dynamic range, and leak. The use of acoustic liquid handling allows for data—both positive and negative—to be quickly generated, screening >900 aTFs through the construction of >3500 reactions in a single day. Through iterative rounds of mutagenesis, we engineer the PbrR protein to detect lead at the lower EPA legal limit of 10 ppb (54 nM), noting selectivity is reduced. Looking forward, we anticipate that the generalized platform reported here could lead to more agile, modular, and bioprogrammable sensors for numerous water and environmental contaminants.

## RESULTS AND DISCUSSION

**Wild-Type PbrR Sensitivity in Cell-Free Reactions Is Insufficient for Diagnostic Application.** We first demonstrated that PbrR can regulate cell-free transcription in the presence of lead. PbrR is a transcriptional activator in the MerR family that, upon ligand binding, has been shown to bind to its cognate operator site (PbrO) and initiate transcription of a downstream reporter (Figure 1A).[21] To test the compatibility


https://doi.org/10.1021/acssynbio.4c00456
ACS Synth. Biol. 2024, 13, 3003−3012

of this system in CFE, we chose to use the fluorescent reporter superfolder green fluorescent protein (sfGFP) because it is stable and can be easily quantified on a plate reader. We constructed a CFE reaction that expressed two DNA templates: the strong T7 promoter driving PbrR expression and the PbrO operator controlling the transcription of sfGFP (Figure 1B and Table 1). The native PbrR begins to induce fluorescent protein expression at around 1 $\mu$M lead, with full activation only seen at 10 $\mu$M lead. This LoD is not sensitive enough to detect lead at the 0.054 $\mu$M (10 ppb) standard set by the EPA.

**Table 1. Summary of Plasmids Used in This Manuscript**[a]

| plasmid description | Addgene ID |
|---|---|
| J23119-pHP14-sfGFP | 136942 |
| pT7-PbrR | 167215 |
| pPbrR-sfGFP | 167222 |
| pPbrR-XylE (C23DO) | 167254 |

[a]The T7 promoter sequence (pT7) is TAATACGACTCACATATA. The consensus *Escherichia coli* promoter J23119 was also used.[32]

**Cell-Free Platform for Rapid, Iterative aTF Engineering.** Having identified the LoD of wild-type PbrR, we next set out to engineer the protein sequence−function relationship to improve the sensitivity for lead. To do this, we applied three rounds of mutagenesis aimed at: (i) discovering design rules about the mutable landscape of PbrR and (ii) improving the LoD and dynamic range of PbrR for lead (Figure 1C). First, we performed alanine scanning mutagenesis throughout the PbrR protein to identify 47 mutational hotspots that impact sensor function. Second, we carried out site saturation mutagenesis at these hotspots to explore a library of 893 mutants. Finally, we combined beneficial mutations from site saturation mutagenesis to identify synergistic effects between high-performing single mutants.

We designed a plate-based high-throughput screen to test mutant aTF libraries. This enabled us to assay each unique library aTF against a panel of different lead concentrations and calculate the fold change for each aTF/analyte condition. We used the Echo acoustic liquid handler (termed "Echo" below) to reduce the experimental time, labor, and reagent costs. The Echo transfers nanoliter-volume fluid droplets using acoustic energy. Individual, unique CFE reactions can be assembled through multiple passes on the Echo by layering nano- and microliter volumes of reagents with each pass. For our assay, we used the Echo to first transfer 1 $\mu$L of premixed CFE reagents (e.g., lysate, amino acids, cofactors, energy substrates, etc.) containing a particular concentration of analytes. On a second pass, we transferred 100 nL of our aTF DNA library. This workflow's most time-consuming step is ordering new DNA libraries (~3 days for delivery).

**Alanine Scanning Mutagenesis Targets Novel Residue Targets for Engineering.** Through homology modeling, it is known that PbrR is a homodimer, with each monomer consisting of an N-terminal DNA binding domain, a C-terminal ligand binding domain (LBD), and a dimerization helix that lies between them (Figure 2A).[23] Unfortunately, little is known about the mutability of PbrR. To develop this understanding, we first performed alanine scanning mutagenesis, which enables the study of each amino acid residue's impact on overall protein activity.[24−26] To do this, we created a library of aTFs where each PbrR variant had an alanine substituted for the native amino acid residue and measured each mutant's ability to regulate transcription in the presence of lead. We tested the alanine scan library at lead concentrations of 0, 1, 10, and 100 $\mu$M (Figure 2B and Supporting Information Table 1). At each concentration, we first calculated the fold change, or dynamic range, defined as the concentration of sfGFP synthesized in the presence of lead divided by the concentration in the no-lead control (defined as leak). We then calculated the normalized fold change, defined as the fold change of an aTF at a lead concentration divided by the fold change of the wild type at the same lead concentration. Normalized fold change both allows for relative activities in the assay to be seen more clearly as well as normalizes for any noise associated between assay replicates run on different days. Omitting variants that had an alanine as the native residue, each assay replicate consisted of 564 unique reactions.

From this assay, we selected residues in the protein that led to positive and negative phenotypic changes. We specifically selected 25 hotspots that displayed increased fold change compared to the wild type at 1 $\mu$M lead (Figure 2C). Positive phenotypic changes, such as increased fold change compared to the wild type for low concentrations of lead, could indicate parts of the PbrR structure that are both tolerant to mutation and potentially play a role in dictating activity. Negative phenotypic changes, such as loss of function or decreased fold change for high concentrations of lead, could indicate that the original residue was essential for functionality. Notably, these variants span all domains of the protein (Figure 2E), with five from the LBD, eight in the HTH motif, and ten in the DNA-binding domain (DBD) (Supporting Information Figure S1). We also selected 25 hotspots that led to the loss of function variants; here, displaying reduced fold change at 100 $\mu$M lead (Figure 2D). The selected residues also spanned all domains of the protein (Figure 2E), with six in the LBD, six in the HTH, and 11 in the DBD (Supporting Information Figure S1). As expected, mutations at the three cysteines responsible for ligand binding[22] (C79A, C123A, and C114A) all showed no activity. From this set of 50, we removed duplicates as well as the start and stop codons to finalize 47 unique hotspots that were taken through for site saturation mutagenesis.

**Site Saturation Mutagenesis of Hotspot Residues.** With mutable residues in PbrR at hand, we next sought to engineer more sensitive aTFs by substituting amino acid residues in each of the 47 hotspots. To do this, we performed site saturation mutagenesis, which is a common strategy to both probe and modify protein functionality.[27−29] We constructed a library of all non-native amino acids at the identified 47 positions via PCR, yielding 893 unique aTF sequences. We then assayed all aTF sequences against 0, 0.1, 1, and 10 $\mu$M lead and calculated normalized fold change, as previously described (Figure 3A and Supporting Information Table 2).

As expected, most substitutions yielded a loss of function mutation. However, some mutants performed better than wild-type PbrR at 0.1, 1.0, and 10 $\mu$M lead. Sites with the highest fold-change improvements often had multiple distinct high-performing amino acid substitutions. For example, G128 showed between two- and three-fold activation above the wild-type at 1 $\mu$M lead when substituted with F, I, L, M, V, W, and Y. Similarly, P61, D64, and K104 were flexible to change. A structural cluster of high performing sites is also seen in M60, P61, and D64 in the DBD, which all showed at least two high-


https://doi.org/10.1021/acssynbio.4c00456
ACS Synth. Biol. 2024, 13, 3003−3012

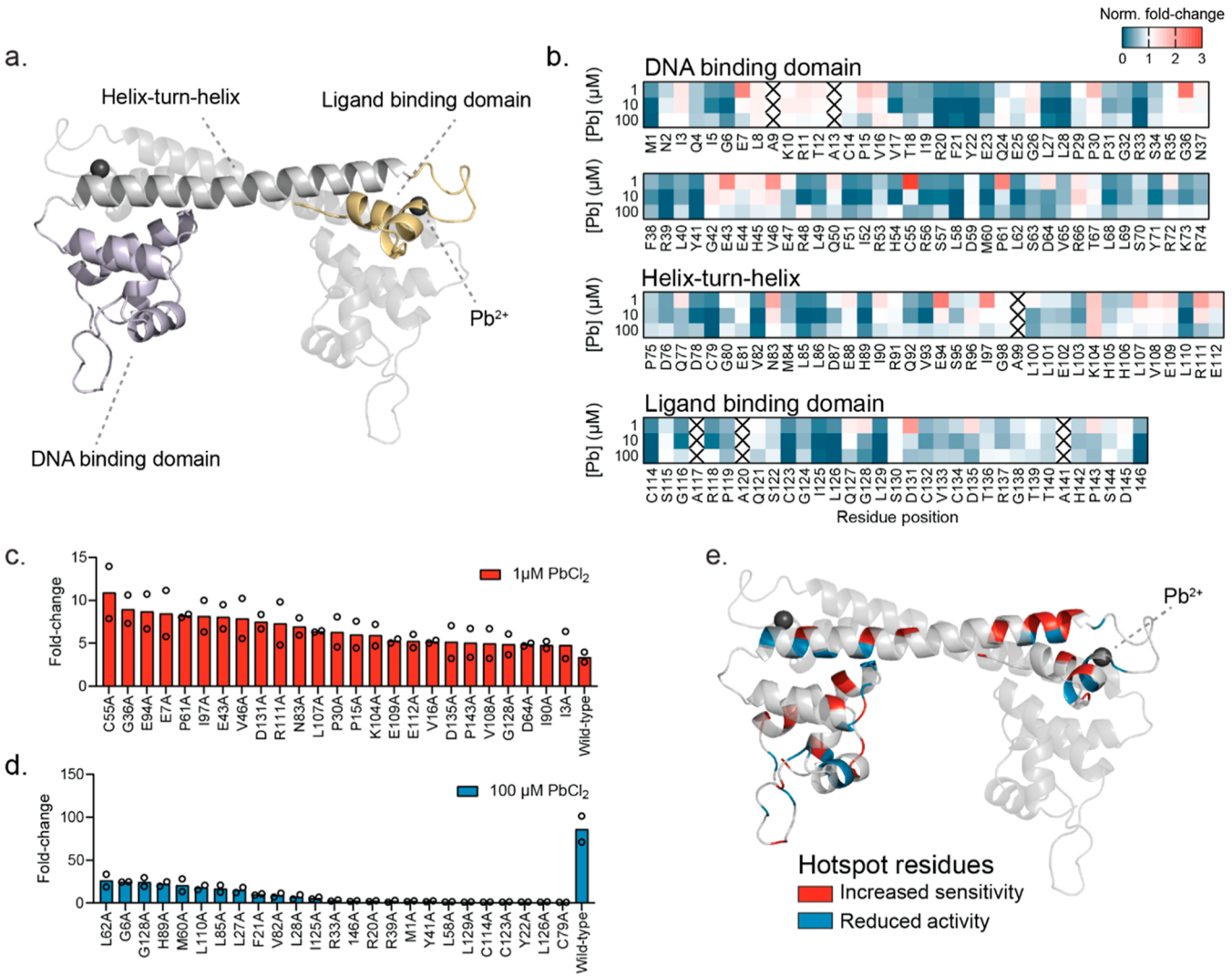


**Figure 2.** Alanine scanning mutagenesis for the identification of hotspots. (A) Predicted PbrR structure depicting the LBD, helix-turn-helix (HTH), and DNA binding domain. Homodimer structure pictured with one monomer highlighted using PyMOL. (B) Alanine scanning mutagenesis library assayed against 0, 1, 10, and 100 $\mu$M Pb to identify sensitivity and loss of function hotspots. Color bar represents normalized fold change (fold change normalized to wild-type fold change for the same ligand condition). Data represent the average between two replicates done on separate days and normalized for each day. Black Xs are residues with native alanine and omitted from the screen. (C) Top 25 sensitivity hotspots selected from the alanine screen. Data are replotted from (B) with bars representing average fold change at 1 $\mu$M Pb between two replicates and individual fold change from each replicate plotted. (D) Top 25 reduced activity hotspots selected from the alanine screen. Data are replotted from (B) with bars representing average fold change at 100 $\mu$M Pb between two replicates and individual fold change from each replicate plotted. (E) Hotspot residues from (C,D) mapped onto the predicted PbrR structure. Red color represents increased sensitivity hotspots and blue represents reduced activity hotspots. Hotspots are only depicted on one monomer.

performing mutants. K104 and L107 in the HTH motif also showed mutants with improved sensitivity.

We next selected the 10 top-performing variants at each lead concentration (21 unique mutants) determined by fold change and validated them by hand (Figure 3B and Supporting Information Figure S2). The top ten variants for 0.1 and 1 $\mu$M lead conditions were almost identical, with D64F, D64K, D64 V, G128M, L107A, and L107C being shared. P61N was the only variant to rank at the top of each lead condition. One reason for low overlap could be that those selected from the 10 $\mu$M lead condition have improved dynamic range rather than an improved affinity or sensitivity for lead. This could be through several mechanisms such as better allostery, stability, or DNA binding that would enable a stronger signal at the same affinity. The top 5 single mutants, defined as highest fold change at 1 $\mu$M lead with repeated residue sites omitted, were G128I, K104 V, P61N, M60L, and D64K.

**Combining Single Mutations into Higher-Order Variants.** We then aimed to engineer sensitivity of PbrR further by combining the top-five single mutants into multisite variants. In addition, we wished to rationally design a K104 V_L107A double mutant due to its high performance determined in the saturation mutagenesis and the proximity of the two residues in PbrR's structure. In total, 27 PbrR mutant combinations were assayed at 0, 0.1, and 0.5 $\mu$M lead (Figure 4A and Supporting Information Table 3). We observed a major shift in population fold change at 1 $\mu$M lead compared with the alanine scan and single saturation mutagenesis libraries (Figure 4B). We ranked the mutants based on fold change at the most sensitive lead condition, 0.1 $\mu$M, and validated them by hand at the full 10 $\mu$L CFE reaction volume


https://doi.org/10.1021/acssynbio.4c00456
ACS Synth. Biol. 2024, 13, 3003−3012

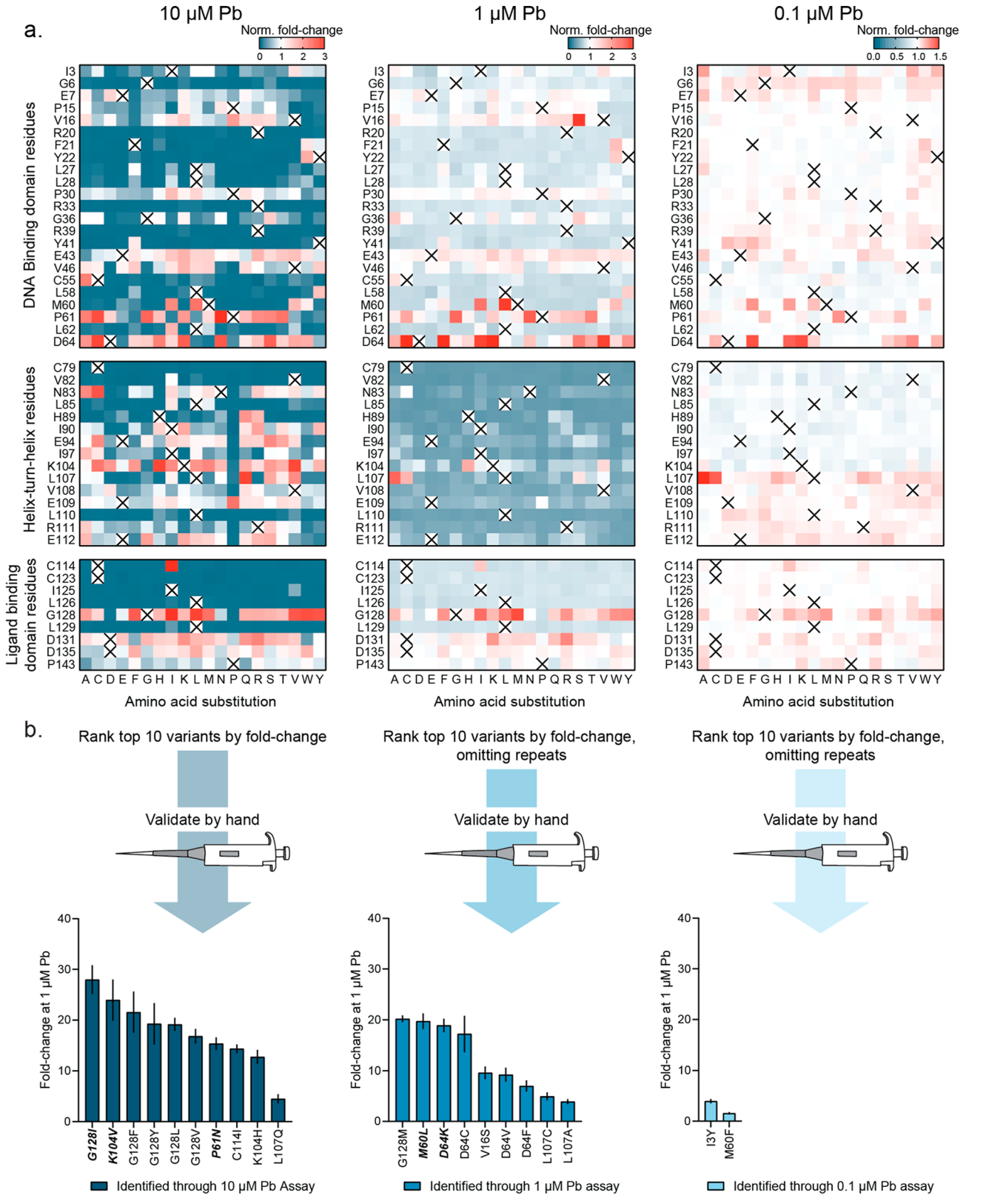


**Figure 3.** Site saturation mutagenesis assay to engineer PbrR sensitivity. (A) PbrR library assayed against 0, 0.1, 1, and 10 $\mu$M led to identify sensitivity mutants. Scale bar represents normalized fold change (fold change normalized to wild-type fold change for the same ligand condition). Data represents either a single replicate or the average between two replicates done on separate days (due to Echo misfires) and normalized for each day. Black Xs are residues with native amino acid identity and were omitted from the screen. (B) Validation of top assay variants at each lead concentration by hand at a standard 10 $\mu$L scale. The 10 variants with the largest fold change were taken through for hand validation from highest to lowest assay lead condition. Repeats that were identified through a previous lead concentration were omitted. Graphed data represents the ratio between average fluorescence with 1 $\mu$M lead divided by average fluorescence in the absence of lead. Error bars are propagated error.



https://doi.org/10.1021/acssynbio.4c00456
ACS Synth. Biol. 2024, 13, 3003−3012

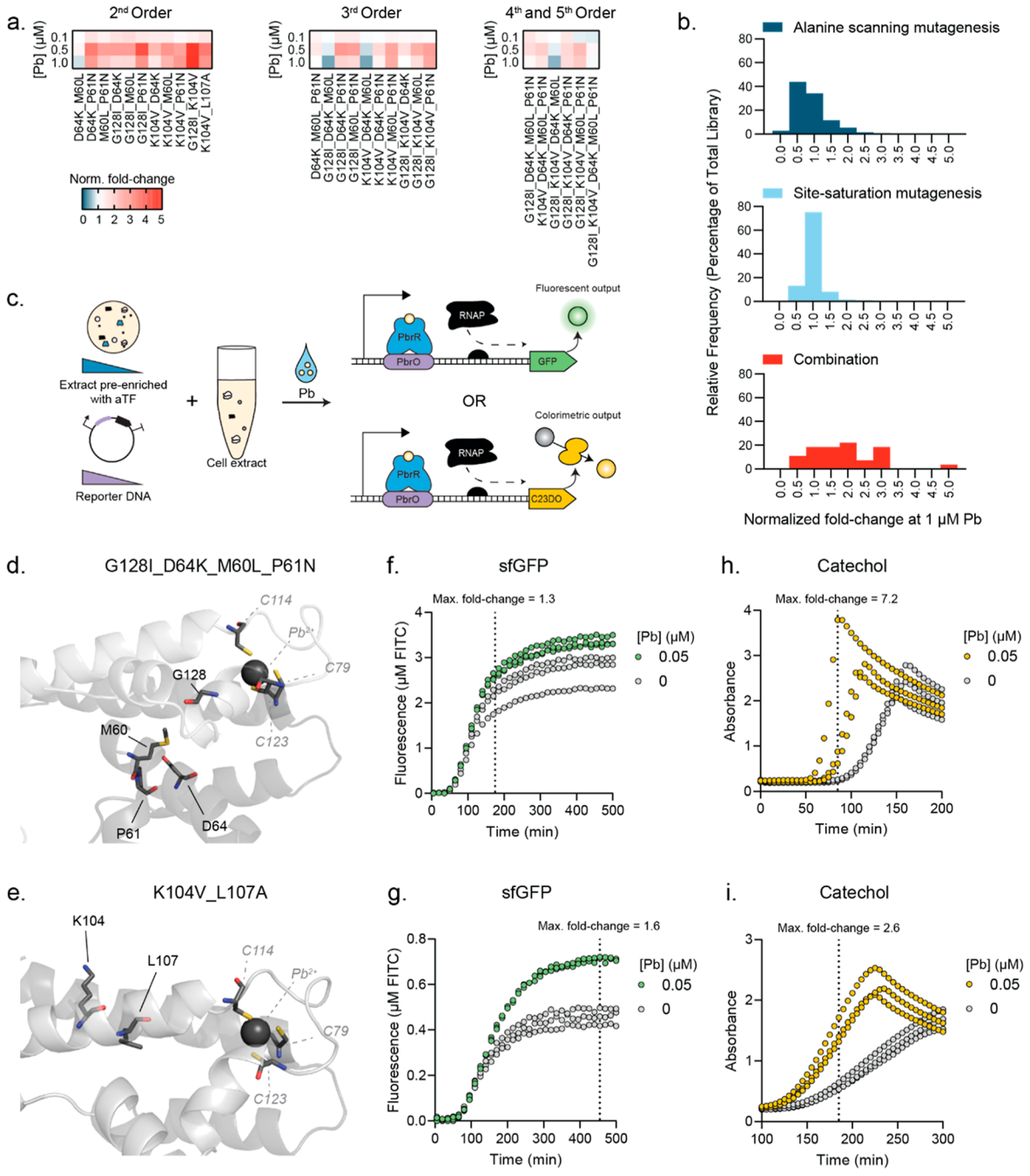


**Figure 4.** Detection of lead at the legal limit achieved by combining PbrR mutants and optimizing the cell-free biosensor format. (A) Top site saturation mutagenesis variants are combined into all 2nd, 3rd, 4th, and 5th order variants and assayed at 0, 0.1, 0.5, and 1 $\mu$M Pb. Scale bar represents normalized fold change (fold change normalized to wild-type fold change for the same ligand condition). Data represent the average between two replicates done on separate days and normalized for each day. (B) Histograms showing the trends in activity at 1 $\mu$M Pb across the alanine scan, site saturation mutagenesis, and combination libraries. Graphed data represents average normalized fold change at 1 $\mu$M Pb as plotted in previous assay figures on the *x* axis. The *y* axis is the relative frequency, reported as a percentage of the total library population. (C) Schematic showing the reaction format optimizations pursued. aTFs were pre-enriched in lysate through expression in the host strain before extract preparation. Reporter DNA concentration was titrated. Both fluorescent (GFP) reporters and colorimetric catechol 2,3-dioxygenase (C23DO) reporters were tested. For the catechol reporter, the C23DO enzyme is produced, cleaving colorless catechol into the yellow pigment 2-hydroxymuconate semialdehyde. (D) G128_D64K_M60L_P61N original residues are highlighted on the PbrR structure. Metal-binding cysteines C114, C79, and C123, as well as the lead ion, are labeled in gray for reference. (E) Kinetic activity of G128I_D64K_M60L_P61N pre-enriched in the extract and tested at 0.05 and 0 $\mu$M lead with a GFP reporter. Each line represents one of three technical triplicates. (F) Kinetic activity of G128I_D64K_M60L_P61N pre-enriched in the extract and tested at 0.05 and 0 $\mu$M lead with a catechol reporter. Each line represents one of three technical triplicates. (G) K104 V_L107A original residues are highlighted on the PbrR structure. Metal-binding cysteines C114, C79, and C123, as well as the lead ion, are labeled in gray for reference. (H) Kinetic activity of K104 V_L107A pre-enriched in the extract and tested at 0.05 and 0 $\mu$M lead with a GFP reporter. Each line represents one of three technical triplicates. (I) Kinetic activity of K104 V_L107A pre-enriched in the extract and tested at 0.05 and 0 $\mu$M lead with a catechol reporter. Each line represents one of three technical triplicates.


https://doi.org/10.1021/acssynbio.4c00456
ACS Synth. Biol. 2024, 13, 3003−3012

(Supporting Information Figure S3). All five mutants (G128I_D64K, G128I_M60L, D64K_L107A, K104 V_L107A, and G128I_D64K_M60L_P61N) showed increased leak at 0 $\mu$M lead compared to the wild type. Despite this, they all were able to detect lead above the background at 0.5 $\mu$M. Notably, G128I_D64K and G128I_M60L were able to detect lead above the background at 0.1 $\mu$M.

MerR-type transcription factors have shown promiscuity for a variety of metals.[21] The cross-talk of PbrR with zinc has been studied as well.[20] Given this, we wondered if engineering PbrR to be more sensitive for its cognate ligand, lead, may have resulted in increased promiscuity for similar metal ligands. To test this, we assayed our top-five combination mutants for promiscuity changes against arsenic, cadmium, cobalt, copper, mercury, nickel, and zinc compared to a negative no-ligand control (Supporting Information Figure S4). We found that many mutants had increased promiscuity for non-lead ligands as compared to wild-type PbrR, especially cadmium, mercury, and zinc.

**Biosensor and Reporter Optimization to Detect Lead at the Legal Limit.** We proceeded to modify the biosensor reaction itself to see whether we could achieve detection of lead at the legal limit (0.054 $\mu$M lead). To do this, we used two approaches (Figure 4C). First, we pre-enriched our extract with aTF, rather than expressing it via LET in CFE by expressing our aTF in vivo in our chassis strain prior to extract harvest.[14] We hypothesized that this would shift the visible LoD by allowing all CFE resources to be allocated only to reporter expression. Second, we changed our reporter module from a fluorescence-based reporter to a colorimetric one. The efficacy of colorimetric catechol reporters has been demonstrated in cell-free biosensing reactions.[16,30,31] For our catechol reporter, we placed the PbrO operator site upstream of a catechol 2,3-dioxygenase (C23DO) enzyme sequence. This enzyme cleaves the colorless catechol molecule into 2-hydroxymuconate semialdehyde, a yellow pigment that is visible by the eye.

Enriched extracts were prepared for the top-5 mutants and tested with a fluorescent sfGFP reporter (Supporting Information Figure S5). Of these, G128I_D64K_M60L_P61N (Figure 4D) showed fluorescent signal above background in response to 0.05 $\mu$M lead with a maximum fold change of 1.3 $\pm$ 0.1 at 175 min (Figure 4F). In addition, K104 V_L107A (Figure 4E) also showed signal activation of 0.05 $\mu$M lead with a fluorescent sfGFP output, achieving a maximum fold change of 1.6 $\pm$ 0.1 after 455 min (Figure 4G). These data demonstrate that pre-enriching the extract with aTF was an effective strategy for shifting the LoD compared to coexpressing aTF and reporter in the CFE reaction. Comparatively, wild-type PbrR showed no fold activation above the background at 0.05 $\mu$M lead (Supporting Information Figure S5).

We next investigated whether signal differentiation above the background could be improved with the use of a catechol reporter for these two mutants. For the catechol reporter, both percent volume of the enriched extract and concentration of the reporter plasmid were co-titrated for G128I_D64K_M60L_P61N and K104 V_L107A (Supporting Information Figure S6). Both G128I_D64K_M60L_P61N (Figure 4H) and K104 V_L107A (Figure 4I) showed an improved signal with a catechol reporter at the legal limit of 0.05 $\mu$M lead. Compared to the sfGFP reporter, G128I_D64K_M60L_P61N had greater signal separation and faster response time, with a maximum fold change around 85 min. K104 V_L107A showed a maximum fold change at 185 min. Fold-change activations were larger than twofold in each case. In comparison, wild-type PbrR showed no fold activation at 0.05 $\mu$M with a catechol reporter (Supporting Information Figure S7).

## CONCLUSIONS

In this work, we demonstrated the ability to engineer PbrR to sense lead at the EPA legal limit. To achieve this goal, we developed a CFE assay that leverages liquid handling robotics to screen libraries of PbrR variants against multiple ligands in 384-well microplates. A key feature of this screen is the ability to quantify both loss of function and gain of function phenotypes. This proved to be essential, as one of the best variants, G128I_D64K_M60L_P61N, was constructed from mutable sites identified through both sensitivity and loss of function hotspots in the initial alanine screen. Furthermore, the open reaction environment of CFE systems combined with automated liquid handling robots enabled a comprehensive mapping of the sequence−function landscape. Most hotspots could not have been identified through structural analysis or canonical strategies alone. For example, most attempts to engineer aTF activity focus on the LBD; however, only one of our top single mutants from the site saturation mutagenesis screen was a ligand-binding domain mutation. Of note, while aTF engineering efforts increased sensitivity, they also lowered selectivity (i.e., sensor activity in the presence of similar, nontarget ligands, Supporting Information Figure S4). In the future, PbrR could be coevolved for both sensitivity and selectivity to address this issue.

Looking forward, we anticipate that the ability to rapidly link the genetic sequence of a given biosensor variant to its corresponding sensory functions (e.g., LoDs, dynamic range, and altered specificity) will be of great utility for the design and optimization of new biosensors for the practical goals of environmental detection and human performance. By leveraging the speed and multiplexed nature of CFE systems for optimizing aTF-promoter pairs for specific analytes, a large search space of variables for optimized sensor modules can be screened that can be ported into diagnostics and implemented in the field.

## METHODS

**DNA Assembly and Purification.** The alanine scanning mutagenesis library was purchased from Twist Biosciences. The SSM and combination mutant libraries were ordered from Integrated DNA Technologies (IDT) as eBlocks with a homology to the pJL1 backbone. The pJL1 backbone was ordered from IDT as a chemically synthesized backbone to prevent plasmid contamination. The eBlocks were assembled into plasmids using standard Gibson Assembly methods with a 15 min incubation at 50 °C. A list of all plasmids, including descriptions and Addgene accession IDs, is presented in Table 1.

**Cell Extract Preparation.** We prepared the extract for optimization of endogenous transcriptional machinery as described previously.[33] In summary, we grew BL21 Star (DE3) (Thermo Fisher Scientific C601003) in 2xYTP media (composed of 16 g/L tryptone, 10 g/L yeast extract, 5 g/L sodium chloride, 7 g/L potassium phosphate dibasic, and 3 g/L potassium phosphate monobasic) adjusted to pH 7.2 with


https://doi.org/10.1021/acssynbio.4c00456
ACS Synth. Biol. 2024, 13, 3003−3012

acetic acid. The strain was grown to an optical density of 0.5 at 37 °C shaking at 250 rpm before induction with isopropyl β-D-1-thiogalactopyranoside to a final concentration of 100 mM and then grown to an optical density of 3.0. We used a 15 min spin at 5000*g* at 4 °C to pellet cells and then washed with 25 mL of wash buffer (14 mM magnesium glutamate, 60 mM potassium glutamate, 10 mM of Tris base, brought to pH 7.8) three times. Cell lysis was performed on an Avestin EmulsiFlex-B15 homogenizer at 24,000 PSI. Cell debris was pelleted by a 10 min spin at 12,000*g* at 4 °C and the clarified lysate was incubated at 37 °C with shaking at 250 rpm for 1 h. We then spun the lysate again at 12,000*g* for 10 min at 4 °C and then dialyzed using a 10K MWCO dialysis membrane (Thermo Fischer Scientific 66380) in dialysis buffer (14 mM magnesium glutamate, 60 mM potassium glutamate, 5 mM Tris base, 1 mM DTT, brought to pH 8.0) for 3 h at 4 °C. After dialysis, the lysate was centrifuged at 12,000*g* for 10 min at 4 °C and the supernatant was flash-frozen on liquid nitrogen and stored at −80 °C.

**Cell-Free Expression Reaction.** CFE reactions were constructed as described elsewhere.[33] In summary, the following component concentrations were assembled together based on previous works:[34−36] 8 mM magnesium glutamate, 10 mM ammonium glutamate, 130 mM potassium glutamate, 1.2 mM ATP, 0.5 mM of CTP, GTP, and UTP respectively, 0.17 mg/mL of *Escherichia coli* MRE600 tRNA (Roche 10109541001), 100 mM NAD, 50 mM CoA, 5 mM oxalic acid, 1 mM spermidine, 1 mM putrescine, 57 mM HEPES at a pH of 7.2, 33.3 mM PEP, 2 mM of each amino acid, and 20% v/v *E. coli* extract, prepared as described above. Water and DNA were used to constitute the rest of the reaction volume. By hand, manual reactions were set up as 10 μL reactions in 384-well clear bottom plates (Corning 3712). Echo-assembled reactions were set up in 384-well V-bottom plates (Bio-Rad HSP3805). Reactions were incubated at 30 °C for 15 h and read on the BioTek Synergy H1 plate reader with excitation of 485 and emission of 528 wavelengths. Fluorescence was quantified by fluorescein isothiocyanate (FITC) standard curves (Sigma-Aldrich 46950). FITC standard curve dilutions were prepared using 50 mM sodium borate at pH 8.5. Lead stocks were prepared from lead chloride powder (Sigma-Aldrich 268690) and diluted using water. All lead concentrations used in the study were validated by the Thermo iCAP Q Inductively Coupled Plasma Spectrometer from the Northwestern Quantitative Bioelement Imaging Center using their standard protocols.

**Echo-Assisted Assembly of Cell-Free Expression Reactions.** Building off previous works,[37,38] two Echo Acoustic Liquid Handlers were used in this study, the 525 (LabCyte 001-10080) and 550 (LabCyte 001-2000). Bulk CFE reagents (not including DNA) were transferred using an Echo Qualified 384-Well Polypropylene 2.0 Plus Microplate on the BP setting (LabCyte PP-0200). aTF DNA in the form of LETs was dispensed from the Echo Qualified 384-well Cyclic Olefin Copolymer (COC) Low Dead Volume Microplate on the 525 (Beckman Coulter 001-13070) and using the Echo Qualified 384-Well Low Dead Volume Microplate plate on the 550 (LabCyte LP-0200). Reactions were programmed on the Echo using either Plate Reformat or CherryPick software.

**Data Analysis and Statistics.** Replicate numbers are described in the associated figure legends. Generally, reactions set up by hand at 10 μL had at least 2 technical replicates per reaction, and individual data points were plotted. Graphs were generated using the GraphPad Prism 9 software, and statistical methods were also performed using built-in GraphPad Prism 9 software as well. The alanine scanning mutagenesis assay and combination variant assays had two replicates. The site saturation mutagenesis assay has one full replicate and one replicate of 868/940 total reactions due to Echo dispense errors. Due to the thorough hand validation of site saturation mutagenesis variants that followed, we accepted the partial replicate.

## ■ ASSOCIATED CONTENT

### Data Availability Statement

Alanine scanning mutagenesis, site saturation mutagenesis, and combination library assay data are provided in the supplement. Source data for all other figures will be available upon request.

### Supporting Information

The Supporting Information is available free of charge at https://pubs.acs.org/doi/10.1021/acssynbio.4c00456.

Alanine scanning mutagenesis library, site saturation mutagenesis library, and combination library assay data (XLSX)

Data describing the distribution of hotspots by protein domain; validations of site saturation mutagenesis and combination variant libraries; promiscuity of top combination variants; enriched extract optimizations; catechol reporter optimizations; and wild-type PbrR baseline experiments (PDF)

## ■ AUTHOR INFORMATION


### Corresponding Author

**Michael C. Jewett** − *Department of Chemical and Biological Engineering, Northwestern University, Evanston, Illinois 60208, United States; Chemistry of Life Processes Institute and Center for Synthetic Biology, Northwestern University, Evanston, Illinois 60208, United States; Robert H. Lurie Comprehensive Cancer Center and Simpson Querrey Institute, Northwestern University, Chicago, Illinois 60611, United States; Department of Bioengineering, Stanford University, Stanford, California 94305, United States;* orcid.org/0000-0003-2948-6211; Email: mjewett@stanford.edu

### Authors

**Holly M. Ekas** − *Department of Chemical and Biological Engineering, Northwestern University, Evanston, Illinois 60208, United States; Chemistry of Life Processes Institute and Center for Synthetic Biology, Northwestern University, Evanston, Illinois 60208, United States;* orcid.org/0009-0007-2487-7287

**Brenda Wang** − *Department of Chemical and Biological Engineering, Northwestern University, Evanston, Illinois 60208, United States; Chemistry of Life Processes Institute and Center for Synthetic Biology, Northwestern University, Evanston, Illinois 60208, United States*

**Adam D. Silverman** − *Department of Chemical and Biological Engineering, Northwestern University, Evanston, Illinois 60208, United States; Chemistry of Life Processes Institute and Center for Synthetic Biology, Northwestern University, Evanston, Illinois 60208, United States;* orcid.org/0000-0002-1990-6609

**Julius B. Lucks** − *Department of Chemical and Biological Engineering, Northwestern University, Evanston, Illinois*




https://doi.org/10.1021/acssynbio.4c00456
ACS Synth. Biol. 2024, 13, 3003−3012

*60208, United States; Chemistry of Life Processes Institute, Center for Synthetic Biology, and Center for Engineering Sustainability and Resilience, Northwestern University, Evanston, Illinois 60208, United States;* orcid.org/0000-0002-0619-6505

**Ashty S. Karim** − *Department of Chemical and Biological Engineering, Northwestern University, Evanston, Illinois 60208, United States; Chemistry of Life Processes Institute and Center for Synthetic Biology, Northwestern University, Evanston, Illinois 60208, United States;* orcid.org/0000-0002-5789-7715

Complete contact information is available at: https://pubs.acs.org/10.1021/acssynbio.4c00456

### Author Contributions

[▽]H.M.E. and B.W. have contributed equally to this work. H.M.E., A.D.S, J.B.L., A.S.K., and M.C.J. conceived this project. H.M.E. and B.W. planned experiments, prepared reagents, performed experiments, and analyzed the data. A.S.K. and M.C.J. supervised the research. H.M.E., A.S.K, J. B. L., and M.C.J. contributed to the writing of the manuscript.

### Notes

The authors declare the following competing financial interest(s): M.C.J. is a co-founder and has financial interest in Stemloop, Inc., Pearl Bio, Gauntlet Bio, and Synolo Therapeutics; J.B.L. is a co-founder and has financial interest in Stemloop. Inc. These interests are reviewed and managed by Northwestern University and Stanford University in accordance with their conflict-of-interest policies. All other authors report no competing interests.

## ■ ACKNOWLEDGMENTS

This work was supported by the Army Research Laboratory and the Army Research Office (W911NF-23-1-0334 and W911NF-22-2-0246), AFOSR (FA9550-23-1-0420), and National Science Foundation (2319427 and 2310382 to J.B.L.). J.B.L. was supported by a John Simon Guggenheim Fellowship. H.M.E. was supported by a National Defense Science and Engineering Graduate Research Fellowship (F-6669029987) and Paul and Daisy Soros Fellowship for New Americans. B.M.W. was supported by a National Science Graduate Research Fellowship (DGE-2234667).

## ■ REFERENCES

(1) Wu, D.; Hu, Y.; Cheng, H.; Ye, X. Detection Techniques for Lead Ions in Water: A Review. *Molecules* **2023**, *28*, 3601.
(2) World Health Organization. *Chemicals of Public Concerns I Lead.*
(3) U.S. Environmental Protection Agency. *Lead Service Lines*, Overviews and Factsheets, 2023.
(4) Huynh, B. Q.; Chin, E. T.; Kiang, M. V. Estimated Childhood Lead Exposure From Drinking Water in Chicago. *JAMA Pediatr.* **2024**, *178*, 473−479.
(5) 40 CFR Part 141 Subpart I-Control of Lead and Copper.
(6) Silverman, A. D.; Karim, A. S.; Jewett, M. C. Cell-free gene expression: an expanded repertoire of applications. *Nat. Rev. Genet.* **2020**, *21*, 151−170.
(7) Carlson, E. D.; Gan, R.; Hodgman, C. E.; Jewett, M. C. Cell-free protein synthesis: Applications come of age. *Biotechnol. Adv.* **2012**, *30*, 1185−1194.
(8) Garenne, D.; Haines, M. C.; Romantseva, E. F.; Freemont, P.; Strychalski, E. A.; Noireaux, V. Cell-free gene expression. *Nat. Rev. Methods Primers* **2021**, *1*, 49.
(9) Tinafar, A.; Jaenes, K.; Pardee, K. Synthetic Biology Goes Cell-Free. *BMC Biol.* **2019**, *17*, 64.
(10) Hunt, J. P.; Zhao, E. L.; Free, T. J.; Soltani, M.; Warr, C. A.; Benedict, A. B.; Takahashi, M. K.; Griffitts, J. S.; Pitt, W. G.; Bundy, B. C. Towards detection of SARS-CoV-2 RNA in human saliva: A paper-based cell-free toehold switch biosensor with a visual bioluminescent output. *New Biotechnol.* **2022**, *66*, 53−60.
(11) Pardee, K.; Green, A. A.; Takahashi, M. K.; Braff, D.; Lambert, G.; Lee, J. W.; Ferrante, T.; Ma, D.; Donghia, N.; Fan, M.; Daringer, N. M.; Bosch, I.; Dudley, D. M.; O'Connor, D. H.; Gehrke, L.; Collins, J. J. Rapid, Low-Cost Detection of Zika Virus Using Programmable Biomolecular Components. *Cell* **2016**, *165*, 1255−1266.
(12) Pardee, K.; Green, A. A.; Ferrante, T.; Cameron, D. E.; Daleykeyser, A.; Yin, P.; Collins, J. J. Paper-based synthetic gene networks. *Cell* **2014**, *159*, 940−954.
(13) Gahlaut, A.; Kharewal, T.; Verma, N.; Hooda, V. Cell-free arsenic biosensors with applied nanomaterials: critical analysis. *Environ. Monit. Assess.* **2022**, *194*, 525.
(14) Silverman, A. D.; Akova, U.; Alam, K. K.; Jewett, M. C.; Lucks, J. B. Design and Optimization of a Cell-Free Atrazine Biosensor. *ACS Synth. Biol.* **2020**, *9*, 671−677.
(15) Jung, J. K.; Alam, K. K.; Verosloff, M. S.; Capdevila, D. A.; Desmau, M.; Clauer, P. R.; Lee, J. W.; Nguyen, P. Q.; Pastén, P. A.; Matiasek, S. J.; Gaillard, J.-F.; Giedroc, D. P.; Collins, J. J.; Lucks, J. B. Cell-free biosensors for rapid detection of water contaminants. *Nat. Biotechnol.* **2020**, *38*, 1451−1459.
(16) Thavarajah, W.; Silverman, A. D.; Verosloff, M. S.; Kelley-Loughnane, N.; Jewett, M. C.; Lucks, J. B. Point-of-Use Detection of Environmental Fluoride via a Cell-Free Riboswitch-Based Biosensor. *ACS Synth. Biol.* **2020**, *9*, 10−18.
(17) Meyer, A. J.; Segall-Shapiro, T. H.; Glassey, E.; Zhang, J.; Voigt, C. A. Escherichia coli "Marionette" strains with 12 highly optimized small-molecule sensors. *Nat. Chem. Biol.* **2019**, *15*, 196−204.
(18) Snoek, T.; Chaberski, E. K.; Ambri, F.; Kol, S.; Bjørn, S. P.; Pang, B.; Barajas, J. F.; Welner, D. H.; Jensen, M. K.; Keasling, J. D. Evolution-guided engineering of small-molecule biosensors. *Nucleic Acids Res.* **2020**, *48*, No. e3.
(19) Machado, L. F. M.; Currin, A.; Dixon, N. Directed evolution of the PcaV allosteric transcription factor to generate a biosensor for aromatic aldehydes. *J. Biol. Eng.* **2019**, *13*, 91.
(20) Jia, X.; Ma, Y.; Bu, R.; Zhao, T.; Wu, K. Directed evolution of a transcription factor PbrR to improve lead selectivity and reduce zinc interference through dual selection. *AMB Express* **2020**, *10*, 67.
(21) Brown, N. L.; Stoyanov, J. V.; Kidd, S. P.; Hobman, J. L. The MerR family of transcriptional regulators. *FEMS Microbiol. Rev.* **2003**, *27*, 145−163.
(22) Hobman, J. L.; Julian, D. J.; Brown, N. L. Cysteine coordination of Pb(II) is involved in the PbrR-dependent activation of the lead-resistance promoter, PpbrA, from Cupriavidus metallidurans CH34. *BMC Microbiol.* **2012**, *12*, 109.
(23) Tolbatov, I.; Re, N.; Coletti, C.; Marrone, A. Determinants of the Lead(II) Affinity in pbrR Protein: A Computational Study. *Inorg. Chem.* **2020**, *59*, 790−800.
(24) Ashkenazi, A.; Presta, L. G.; Marsters, S. A.; Camerato, T. R.; Rosenthal, K. A.; Fendly, B. M.; Capon, D. J. Mapping the CD4 binding site for human immunodeficiency virus by alanine-scanning mutagenesis. *Proc. Natl. Acad. Sci. U.S.A.* **1990**, *87*, 7150−7154.
(25) Morrison, K. L.; Weiss, G. A. Combinatorial alanine-scanning. *Curr. Opin. Chem. Biol.* **2001**, *5*, 302−307.
(26) Reimer, A.; Maffenbeier, V.; Dubey, M.; Sentchilo, V.; Tavares, D.; Gil, M. H.; Beggah, S.; Van Der Meer, J. R. Complete alanine scanning of the Escherichia coli RbsB ribose binding protein reveals residues important for chemoreceptor signaling and periplasmic abundance. *Sci. Rep.* **2017**, *7*, 8245−8311.
(27) Siloto, R. M. P.; Weselake, R. J. Site saturation mutagenesis: Methods and applications in protein engineering. *Biocatal. Agric. Biotechnol.* **2012**, *1*, 181−189.
(28) Andrews, F. H.; McLeish, M. J. Using site-saturation mutagenesis to explore mechanism and substrate specificity in

thiamin diphosphate-dependent enzymes. *FEBS J.* **2013**, *280*, 6395−6411.
(29) Parikh, M. R.; Matsumura, I. Site-saturation Mutagenesis is more Efficient than DNA Shuffling for the Directed Evolution of β-Fucosidase from β-Galactosidase. *J. Mol. Biol.* **2005**, *352*, 621−628.
(30) Liu, X.; Silverman, A. D.; Alam, K. K.; Iverson, E.; Lucks, J. B.; Jewett, M. C.; Raman, S. Design of a Transcriptional Biosensor for the Portable, On-Demand Detection of Cyanuric Acid. *ACS Synth. Biol.* **2020**, *9*, 84−94.
(31) Thavarajah, W.; Owuor, P. M.; Awuor, D. R.; Kiprotich, K.; Aggarwal, R.; Lucks, J. B.; Young, S. L. The accuracy and usability of point-of-use fluoride biosensors in rural Kenya. *npj Clean Water* **2023**, *6*, 5−8.
(32) Kelly, J. R.; Rubin, A. J.; Davis, J. H.; Ajo-Franklin, C. M.; Cumbers, J.; Czar, M. J.; de Mora, K.; Glieberman, A. L.; Monie, D. D.; Endy, D. Measuring the activity of BioBrick promoters using an in vivo reference standard. *J. Biol. Eng.* **2009**, *3*, 4.
(33) Silverman, A. D.; Kelley-Loughnane, N.; Lucks, J. B.; Jewett, M. C. Deconstructing Cell-Free Extract Preparation for in Vitro Activation of Transcriptional Genetic Circuitry. *ACS Synth. Biol.* **2019**, *8*, 403−414.
(34) Kwon, Y.-C.; Jewett, M. C. High-throughput preparation methods of crude extract for robust cell-free protein synthesis. *Sci. Rep.* **2015**, *5*, 8663.
(35) Jewett, M. C.; Calhoun, K. A.; Voloshin, A.; Wuu, J. J.; Swartz, J. R. An integrated cell-free metabolic platform for protein production and synthetic biology. *Mol. Syst. Biol.* **2008**, *4*, 220.
(36) Jewett, M. C.; Swartz, J. R. Mimicking the Escherichia coli cytoplasmic environment activates long-lived and efficient cell-free protein synthesis. *Biotechnol. Bioeng.* **2004**, *86*, 19−26.
(37) Hunt, A. C.; Vögeli, B.; Hassan, A. O.; Guerrero, L.; Kightlinger, W.; Yoesep, D. J.; Krüger, A.; DeWinter, M.; Diamond, M. S.; Karim, A. S.; Jewett, M. C. A rapid cell-free expression and screening platform for antibody discovery. *Nat. Commun.* **2023**, *14*, 3897.
(38) Hunt, A. C.; Case, J. B.; Park, Y.-J.; Cao, L.; Wu, K.; Walls, A. C.; Liu, Z.; Bowen, J. E.; Yeh, H.-W.; Saini, S.; Helms, L.; Zhao, Y. T.; Hsiang, T.-Y.; Starr, T. N.; Goreshnik, I.; Kozodoy, L.; Carter, L.; Ravichandran, R.; Green, L. B.; Matochko, W. L.; Thomson, C. A.; Vögeli, B.; Krüger, A.; VanBlargan, L. A.; Chen, R. E.; Ying, B.; Bailey, A. L.; Kafai, N. M.; Boyken, S. E.; Ljubetič, A.; Edman, N.; Ueda, G.; Chow, C. M.; Johnson, M.; Addetia, A.; Navarro, M.-J.; Panpradist, N.; Gale, M.; Freedman, B. S.; Bloom, J. D.; Ruohola-Baker, H.; Whelan, S. P. J.; Stewart, L.; Diamond, M. S.; Veesler, D.; Jewett, M. C.; Baker, D. Multivalent designed proteins neutralize SARS-CoV-2 variants of concern and confer protection against infection in mice. *Sci. Transl. Med.* **2022**, *14*, No. eabn1252.


https://doi.org/10.1021/acssynbio.4c00456
*ACS Synth. Biol.* 2024, 13, 3003−3012